

Development and operation of the twin radio frequency single electron transistor for solid state qubit readout

T. M. Buehler, D. J. Reilly, R. P. Starrett, A. R. Hamilton, A. S. Dzurak and R. G. Clark

*Centre for Quantum Computer Technology, Schools of Physics and Electrical Engineering & Telecommunications,
University of New South Wales, Sydney 2052, Australia*

Operation of a scalable solid state quantum computer requires that readout be efficient and fast. In an effort to meet this objective we have developed a twin radio frequency superconducting single electron transistor device (twin rf-SET) that is capable of distinguishing sub-electron signals from charge noise on microsecond time-scales. The twin rf-SET makes use of two tuned resonance circuits to simultaneously and independently address both rf-SETs using wavelength division multiplexing (WDM) and a single cryogenic amplifier. Here we describe the operation of the twin rf-SET as a charge detector and evaluate the cross-talk between the two resonance circuits. Real time suppression of charge noise is demonstrated by cross correlating the signals from the two rf-SETs. For the case of simultaneous operation, the rf-SETs had charge sensitivities of $4.4\mu e/\sqrt{Hz}$ and $7.5\mu e/\sqrt{Hz}$.

I. INTRODUCTION

Quantum computers are machines that directly harness quantum mechanics to perform information processing [1]. These machines promise to be exceedingly powerful at solving certain problems [2], which are intractable for classical computers. Operation of such a device however, is contingent on the ability to readout the state of a single two-level quantum system (qubit). In recent proposals for scalable solid state architectures [3–5], this formidable challenge amounts to sensing sub-electron charge or flux variation using detectors such as the single electron transistor (SET) or the superconducting quantum interference device (SQUID) [6]. In addition to the requirement of extreme sensitivity, readout devices also need to operate on time-scales less than the qubit mixing time, after which information about the qubit state is lost [7]. Towards this goal, recent experiments [8] have explored the possibility of utilising the radio frequency SET (rf-SET) [9] to perform readout on the time-scales needed for the single-shot measurement of a solid state qubit.

The work presented here describes the development of a *twin* rf-SET device that utilizes two superconducting single electron transistors in simultaneous, independent operation on micro-second time scales. Independent control of the source-drain bias across the SETs permits both devices to simultaneously operate at the point of maximum sensitivity and measurement efficiency. In addition, by making use of wavelength division multiplexing (WDM) the twin rf-SET is capable of providing two (or more) outputs for cross-correlation measurements using only a single cryogenic following amplifier and a single transmission line. The cross-correlation technique is advantageous in suppressing charge noise originating from fluctuating traps in the surrounding material system and constitutes a means of discriminating readout signals from spurious signals [10].

The operation of a SET charge detector is based on the

Coulomb blockade [11] of electrons tunneling across two low capacitance junctions (C_1, R_1 and C_2, R_2). An ‘island’ with a characteristic charging energy $E_C = e^2/2C_\Sigma$, where C_Σ is the capacitive coupling to the environment, is formed between the tunnel junctions. The sequential electron tunneling current across the island can be controlled by the voltage on a gate which is capacitively coupled to the island. Coulomb blockade is effective for temperatures $T < E_C/k_B$ and for tunneling resistances $R_{1,2}$ of order of the resistance quantum $h/e^2 \approx 26k\Omega$. These restrictions generally limit the operation of SETs to cryogenic temperatures. SETs fabricated from metals that exhibit superconductivity at these temperatures generally also display rich current - voltage characteristics in association with the interplay between charging effects and Cooper pair transport. Notably, in the vicinity of the source-drain threshold voltage for current transport (defined by the superconducting gap and the charging energy), resonant tunneling processes can be observed which are governed by the dynamics of coherent Cooper pair and incoherent quasi-particle transport [12]. Superconducting SETs have recently been explored in conjunction with reading-out a quantum computer and shown to approach quantum limits for measurement efficiency [13].

Typical qubit mixing times ($T_{mix} \sim 1 - 10\mu s$) [14] necessitate the use of a fast and sensitive detector. Traditionally, the bandwidth of SETs has been limited to a few kHz by the large RC time constant associated with the SET output impedance and the capacitance of the wiring from the SET to the room temperature amplifiers. In contrast to the conventional SET, the rf-SET [9] makes use of a LC impedance transformer to match the impedance of the SET to the characteristic impedance of a transmission line. In this regime, either the reflected [9] or transmitted [15] power of an incident rf carrier wave is a function of the SET resistance. Mapping the device resistance to changes in the reflected or transmitted power thereby allows fast charge detection. In the case of reflec-

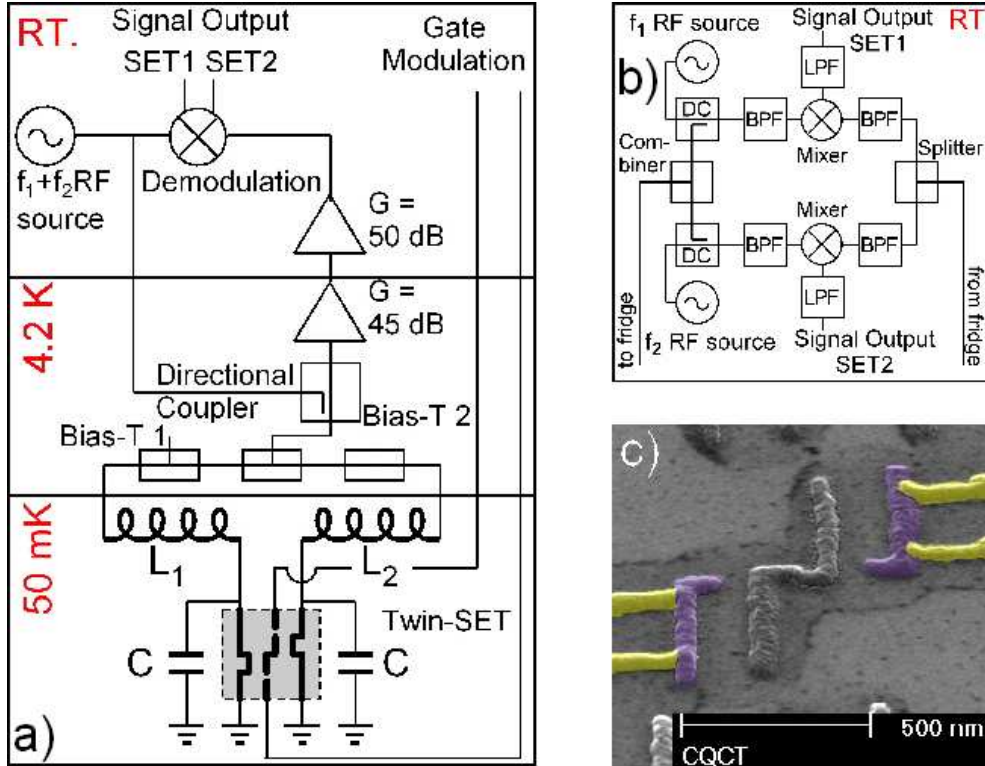


FIG. 1: a) Schematic of the twin rf-SET setup. Signals are coupled to the tank circuits by using a directional coupler and are then directed to the corresponding SET by the tuned impedance transformers. The reflected signal feeds cryogenic (gain = 45dB) and room temperature (gain = 50dB) amplifiers. Two bias-Tees allow independent dc-biasing of each SET. b) Schematic of the rf carrier generation and signal demodulation. The incident carrier wave is produced by combining the output of two independent rf signal generators. c) SEM image of a twin-SET device. The tunnel barriers required for Coulomb blockade are formed after the first evaporation step by in-situ oxidation of the aluminum surface. For SET2 (right) the overlaps of source and drain leads (second evaporation) with the SET island (first evaporation) can be seen.

tion measurements, the incident rf carrier is coupled to the *LCR* matching network via a directional coupler and the reflected power is coupled to a low noise cryogenic amplifier. The *LCR* circuit is described by the loaded quality factor $Q = (Z_{LC}/R_{SET} + Z_0/Z_{LC})^{-1}$, where Z_0 is the characteristic impedance of the transmission line and R_{SET} is the resistance of the SET.

The technique of wavelength division multiplexing has long been applied in communications engineering as a means of utilizing channel resources efficiently. In line with earlier work on SQUIDs [16], recent work by Stevenson *et al.*, [17] has explored the possibility of using multiplexed rf-SETs to amplify signals from high impedance photon detectors for application in astronomy. In contrast to these results, the twin rf-SET device described here is designed specifically as a readout device in a solid state quantum computer. We describe a heterodyne demodulation scheme that enables independent signal detection of both rf-SETs together with *real-time* cross-correlation. This is the first time that sub-electron charge signals have been cross-correlated on microsecond time-scales using rf-SETs.

II. TWIN RF-SET SETUP

Turning now to the specifics of our setup, we achieve multiplexing of signals from the two rf-SETs via two tuned impedance transformers (Figure 1a). Each tank circuit consists of a parasitic capacitance C to ground and a chip inductor with inductance $L_{1,2}$. The circuits are tuned by choosing appropriate inductances to transform the impedance of the SET (typically 40 - 100k Ω) downward towards a characteristic impedance of 50 Ω at the respective resonant frequency $\omega_{1,2} = 1/\sqrt{CL_{1,2}}$. Figure 1a shows a schematic of our cryogenic set-up, including two separate bias-tees for independent dc-biasing of each SET. The length of coaxial transmission line between the 'T' section and the SETs is tuned so that additional reflections are minimized. In the present experimental arrangement we place our cryogenic following amplifier at the 4 K stage of our dilution refrigerator to reduce losses between the SET and the amplifier. The twin rf-SET data presented here was taken using tank circuits with resonance frequencies $f_1 = 335\text{MHz}$ and $f_2 = 360\text{MHz}$, using inductances of 780nH and 660nH, with a total parasitic capacitance estimated to be $\sim 0.3\text{pF}$ for each SET. The choice of frequencies corresponds to the band-

width where our cryogenic rf-amplifier maintains optimum noise performance and in addition, where chip inductors are readily available.

The incident carrier wave is produced by combining the output of two independent rf signal generators (Figure 1b). Each generator output is fed to a directional coupler in order to tap off power (-16dB) for the SETs. The remaining signal (-0.11dB) is directed to the mixers. A subsequent splitter/combiner is used to feed the two frequencies to one semi-rigid coaxial waveguide into the cryostat. After the signal enters the cryostat (Figure 1a) the rf power is coupled to the tank circuits using another directional coupler and directed to the corresponding SET by the tuned impedance transformers. The reflected signal is then coupled to the cryogenic amplifier (45dB gain) and a room temperature amplifier (50dB gain). A power splitter (right side of Figure 1b) feeds the reflected rf signal to two mixers for demodulation. High roll-off, narrow bandpass filters are used before both the local oscillator (LO) and RF mixer inputs to suppress inter-modulation distortion [18] and higher order components. Active phase-shifters are used to ensure constructive interference of RF and LO inputs at the mixer. Finally, the intermediate frequency (IF) mixer product is low-pass filtered before being output into either a multichannel oscilloscope or spectrum analyzer for time and frequency domain measurements respectively. To further improve signal quality we also use various attenuators and filters at room and cryogenic temperatures.

Figure 1c shows a SEM image of an Al/Al_2O_3 twin-SET device used in these experiments. The device was fabricated using electron beam lithography and the standard shadow mask evaporation technique [19]. The tunnel junctions are formed where the leads (horizontal) overlap with the ‘islands’ (vertical). In this arrangement the SETs are ~ 500 nm apart and gates used in these experiments couple to both SETs inducing charges of similar magnitude on both devices. In addition there is a central double-dot structure, developed for readout simulations but not relevant to the measurements described here [10].

III. TANK CIRCUIT CHARACTERISATION

In order to maximize the sensitivity of the rf-SET, the device should be operated in a regime where the amount of reflected power depends most strongly on the SET resistance. We first describe two different modes of operation for a single rf-SET. Figure 2a shows the calculated power reflection coefficient Γ^2 ($\Gamma = (Z_0 - Z_{LCR})/(Z_0 + Z_{LCR})$) as a function of the SET resistance for one matching network. The tank circuit LC values were chosen to transform a $50\text{k}\Omega$ impedance to Z_0 (50Ω) at resonance. For perfect matching the power reflection coefficient then approaches zero when the SET resistance is $50\text{k}\Omega$. We define two modes of operation, the under-matched regime (device resistance greater than $50\text{k}\Omega$ -

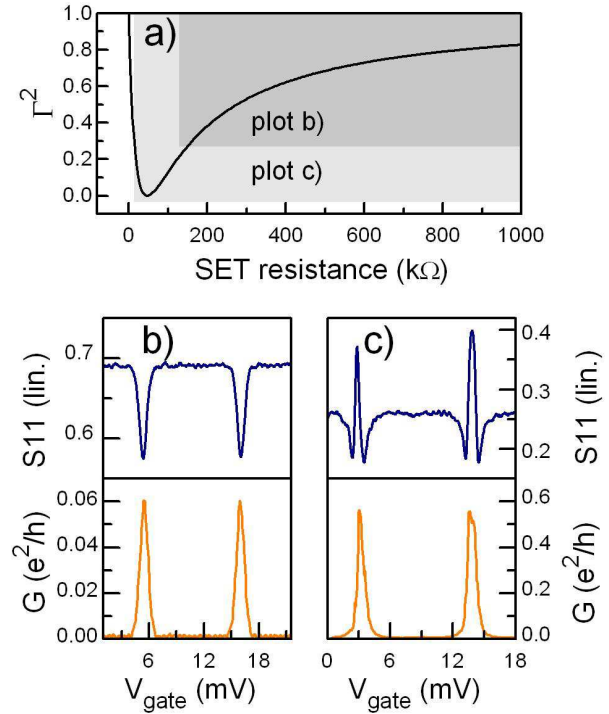


FIG. 2: a) Calculation of the power reflection coefficient as a function of the SET resistance for an impedance transformer designed to match $50\text{k}\Omega$ to $Z_0 = 50\Omega$. The shaded regions correspond to the matching regimes shown in b) and c). b) Reflected rf power (top) and dc conductance (bottom) in the normal state ($B=0.5\text{T}$). The SET resistance remains above $50\text{k}\Omega$ (note the different scale on the y-axis) throughout and the impedance transformer operates in the under-matched regime. c) Reflected rf power (top, S_{11}) and dc conductance (bottom) in the superconducting state. The SET is biased to a region where the resistance at the top of a peak is less than $50\text{k}\Omega$. The non-monotonic dependence on gate bias arises as the operating point moves from under to over matched.

dark grey shaded area in Figure 2a) and the over-matched regime (device resistance smaller than $50\text{k}\Omega$ - light grey shaded area in Figure 2a). Over-matching yields an enhanced depth of modulation in association with the large slope of Γ^2 as a function of the SET resistance.

Figures 2b and 2c show measurement results for a single rf-SET. The reflected rf power (top) is measured together with the dc conductance (bottom) as a function of gate voltage. The data shown in Figure 2b was taken with the SET maintained in the normal state ($B=0.5\text{T}$). The high differential resistance limits operation to the under-matched regime, where the resistance of the SET is always greater than $50\text{k}\Omega$. The corresponding behavior of the reflection coefficient is indicated in Figure 2a by the darker shaded region. In this regime the reflected power increases monotonically with increasing SET resistance, so that the S_{11} data shown in Figure 2b is a

mirror image of the SET conductance. In contrast, the data shown in Figure 2c was taken with the SET in the superconducting state ($B=0$) and biased to a point where the differential resistance approaches the resistance quantum ($\sim 26\text{k}\Omega$) at the top of a Coulomb blockade peak. Moving from the blockaded state to a point where the differential resistance is less than $50\text{k}\Omega$ results in a non-monotonic response in the reflected rf power as shown in the upper section of Figure 2c. This behavior is due to the impedance transformer operating initially in the under-matched regime and moving to over-matching as the differential resistance moves through $50\text{k}\Omega$. This is indicated by the lightly shaded region in Figure 2a. The non-monotonic behavior of the transfer function in the over-matched regime complicates operation of the device as a charge detector, as seen in the upper panel of Figure 2c. The benefit of the increased depth of modulation and sensitivity is compromised by the added requirement for more accurate gate biasing for readout.

We turn now to the operation of a twin-SET charge detector. Independent operation of two rf-SETs requires two tank circuits with different resonance frequencies. The minimum acceptable spacing in frequency is determined by the Q-factor of the tank and the acceptable amount of cross-talk between the two devices. Despite the obvious direct capacitive coupling of the gates to both SETs, we are able to investigate the cross-talk between the resonant circuits by studying the reflected power at *both* resonant frequencies f_1 and f_2 as a function of the SET resistances. Figures 3a and 3b show the calculated voltage signal after demodulation for two different frequency separations of the tank circuits. This voltage signal is proportional to the square root of the reflected power and in turn, the differential resistance of the SET. The solid lines in Figures 3a and 3b show how the calculated output of the SET1 tank circuit (tank1) varies as the resistance of SET1 is varied, with the SET2 resistance fixed at $200\text{k}\Omega$. The dashed lines show how the calculated output of the SET2 tank circuit (tank2) also varies with the resistance of SET1, for several different values of SET2 resistance. At the inflection point of the tank1 curve, the output voltage is zero corresponding to a reflection coefficient Γ of zero, or perfect matching. If there was no cross-coupling between the two circuits, then the output signal for tank2 should be independent of the resistance of SET1, so that the dashed lines would be perfectly horizontal. However, the finite cross-coupling causes the output of tank2 to drop as the resistance of SET1 is reduced, which is particularly noticeable at low SET resistances in the over-matched regime. Figures 3a and 3b are for the cases where the resonance frequencies of the two tank circuits are separated by 20MHz and 50MHz respectively. Comparing Figures 3a and 3b one can see that the calculated cross-talk is reduced as the two resonant frequencies are moved further apart, and as the resistance of the SETs is kept high.

In order to measure the cross-talk experimentally, we monitor the reflected power as a function of frequency, for

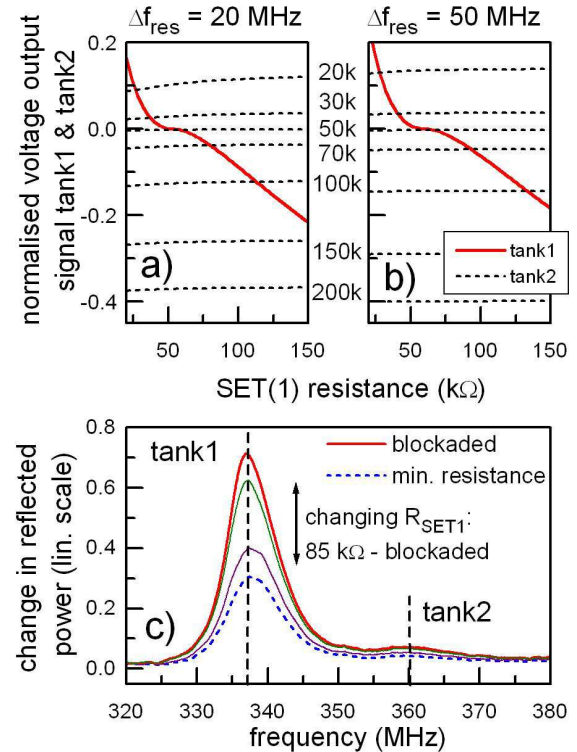


FIG. 3: Effective cross talk between each resonant tank circuit. The output signal from tank1 (solid) and tank2 (near horizontal dashed lines) is calculated and shown as a function of SET1 resistance for resonance separations of **a)** 20MHz and **b)** 50MHz. The resistance of SET2 was stepped from $20\text{k}\Omega$ to $200\text{k}\Omega$. **c)** shows the measured (normalized) reflected power from the two tank circuits as a function of frequency. Cross talk between the two circuits can be seen in the small variation of the signal from tank(2), while the resistance of SET1 is varied over its full dynamic range.

different values of SET1 resistance (Figure 3c). The resistance of SET2 was kept constant by applying a source-drain dc-bias above the threshold voltage for Coulomb blockade (which keeps R_{SET2} fixed at $\sim 40\text{k}\Omega$), while the resistance of SET1 was tuned with the gate bias. The traces shown were normalised with respect to the case where both SETs are dc-biased above the threshold voltage for Coulomb blockade. Figure 3c reveals a small variation in the reflected signal for tank2 as the resistance of SET1 is varied. Changing the resistance of SET1 over its full dynamic range (from $\sim 85\text{k}\Omega$ to $10\text{M}\Omega$) caused a change of about 8% at the resonance frequency of tank2.

Cross-talk between the two tank circuits could be minimised by moving the resonances further apart in frequency. However, in order to minimise the noise temperature of the cryogenic amplifier to achieve the maximum sensitivity of the rf-SET, the amplifier is usually optimised for a relatively narrow bandwidth. This leads to a trade-off between the noise temperature of the amplifier (rf-SET sensitivity), the bandwidth of the SET tank cir-

cuits and the cross-talk between the tank circuits. For a given separation of the resonances, wide bandwidth (low-Q) tank circuits will suffer more from cross-talk than their narrow bandwidth (high-Q) counterparts. This restriction will affect the number of multiplexed SETs that can be simultaneously addressed within the optimal operating bandwidth of the cryogenic amplifier. Despite these restrictions, for the present application (two resonances separated by ~ 20 MHz) the multiplexing technique works well with the SETs very close to independent operation.

IV. SENSITIVITY AND CHARGE NOISE REJECTION

We now discuss measurement results for the twin rf-SET device, beginning with the charge sensitivity for simultaneous operation. The data shown in Figure 4 was taken with the SETs in the superconducting regime. Operating the twin rf-SET in the superconducting mode maximizes the device sensitivity, since the transconductance and small signal differential resistance are maximized in conjunction with a minimum in the shot noise (when operating at the double Josephson quasi-particle peak (DJQP)). The top trace of Figure 4a shows the reflected power measured with a network analyzer, with dips at the two resonances of tank1 and tank2. The lower trace shows frequency domain data for both rf-SETs in response to a 2.5 MHz sine wave signal applied to the gate with a rms amplitude of $\sim 0.1e$. Clear amplitude modulation (AM) of both rf carriers is observed. The sensitivity of the rf-SET can now be determined by measuring the signal to noise ratio (SNR) of either sideband for a rms induced charge signal q_{rms} on the SET island. The minimum charge variation detectable in a measurement time of 1 second is given by [20]:

$$\delta q = \frac{q_{rms}}{\sqrt{B} \times 10^{SNR/20}} (e/\sqrt{Hz}) \quad (1)$$

where B is the chosen resolution bandwidth of the spectrum analyzer. For the twin rf-SET device studied here, we measure an optimum sensitivity of $\delta q = 7.5\mu e/\sqrt{Hz}$ and $\delta q = 4.4\mu e/\sqrt{Hz}$ for SET1 and SET2 with resonances at 335MHz and 360MHz respectively. The sensitivities were measured for $\delta q = 0.005e$ signals at 1.3 MHz in the dc+rf (superconducting) mode [20].

We now present data showing the response of the SETs in the time domain, and demonstrate the suppression of charge noise with the twin rf-SET. Figure 4b shows the response of both SETs (measured simultaneously) when a 1 kHz square wave is applied to a nearby gate via a 40 dB attenuator. This signal induces charges of $\sim 0.1e$ and $\sim 0.05e$ on the islands of SET1 and SET2 respectively. Although the output of the two SETs faithfully follow the gate signal, additional unwanted charge noise is also picked up by SET2 (e.g. in the 0.7 - 1 ms time interval). The observed random telegraph signals (RTSs) are associated with charge noise arising from two-level charge

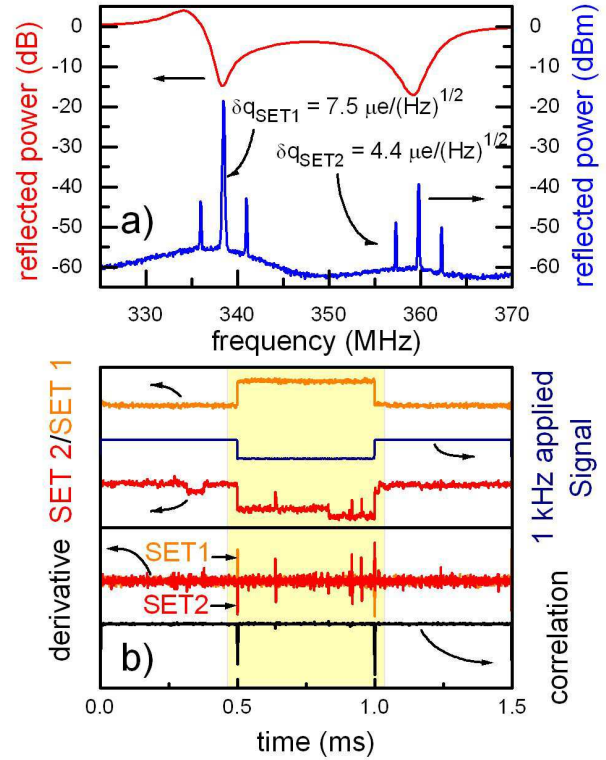


FIG. 4: a) Frequency dependence of the reflected power in dB from both tank circuits as measured with a network analyzer (top trace). The bottom trace shows a typical amplitude modulation (AM) signal associated with both the SETs responding to a $\sim 0.1e$, 2.5MHz gate signal. Charge sensitivities for each device are stated for the case of simultaneous operation (different measurement). b) time domain data taken simultaneously with both SETs. Both devices respond independently to a 1kHz square wave signal applied to a nearby gate. Spurious charge noise is superimposed on the output of SET2 (shown in the highlighted region). By cross-correlating the signals from both SETs (multiplying the derivatives) we are able to suppress spurious charge noise events in real time.

traps in the SET oxide tunnel barrier and substrate. Using a multi-channel digital oscilloscope, we are able to multiply the time derivative signals from SET1 and SET2 in *real-time*. The result is shown in the lower portion of Figure 4b and constitutes a real-time cross-correlation of the SET signals. Close inspection of the correlation trace shows that this technique produces sharp spikes when there is a true signal that affects both SETs (such as the rising or falling edges of the square wave applied to the gate) and a clear suppression of the random charge noise. This ability to reject events associated with charge noise will be important for the application of SETs in the readout of solid state quantum computers.

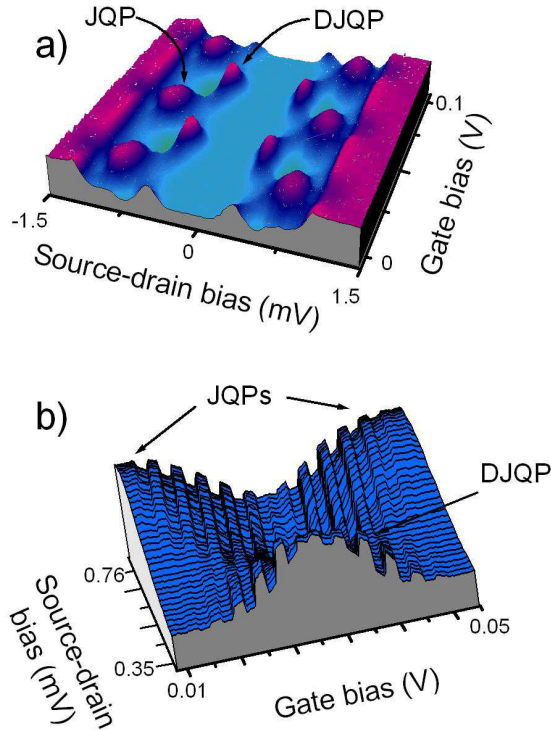


FIG. 5: **a)** Bias spectroscopy for the rf-SET. The rf reflected power is proportional to the differential resistance and is shown on the intensity scale as a function of the source-drain bias and gate voltage. **b)** Zoomed-in region of the intensity plot shown in Figure 5a with the addition of a small signal square wave applied to the gate. The signal amplitude rises as a function of the SET transconductance reaching a maximum at regions associated with resonant Cooper pair tunneling.

V. OPERATING THE RF-SET FOR EFFICIENT QUBIT READOUT

Finally, having addressed the issues affecting charge sensitivity of the twin rf-SET and charge noise rejection, we now discuss how the rf-SET can be operated as a highly efficient detector for qubit readout. In this context efficient readout means that the ratio of the time required to collapse the qubit wavefunction to the measurement time approaches unity ($\tau_\phi/\tau_{meas} < 1$). Recent theoretical work [13] has suggested that a superconducting SET (SSET) biased at the double Josephson quasi-particle peak is a particularly efficient readout device. More significantly for practical radio frequency operation, the differential resistance at this point approaches the resistance quantum ($\sim 26\text{k}\Omega$) regardless of the tunnel junction resistance [21]. Given that the SET tunnel junction resistance is generally not precisely known prior to low temperature measurement, an ability to consistently achieve a constant differential resistance via biasing greatly simplifies the design of the tank circuit.

In our measurement setup both SETs can indepen-

dently be source-drain biased, allowing for optimised operation of both SSETs. We now present data showing the Josephson quasi-particle resonance peaks as a function of gate and source - drain bias for one SET. Figure 5a shows an intensity plot for SET2 where the data was taken using the rf setup outlined above. The amplitude of the demodulated output voltage signal is represented by the intensity scale and reflects the differential resistance (dv/di) as a function of source-drain and gate bias (dark regions represent points of low differential resistance). The middle region of the plot about $V_{SD}=0$ where the device is blockaded due to the superconducting energy gap is light. Moving outward in source - drain bias Coulomb blockade oscillations appear with gate bias, reaching a maximum amplitude at source - drain biases that correspond to Josephson quasi-particle resonances.

The readout efficiency and back-action of the rf-SET are strong functions of the noise spectral density as determined by the dynamics of the resonant tunnelling and thereby of the bias conditions as shown in Figure 5a. To demonstrate how the sensitivity of the rf-SET depends on the gate and source - drain bias when operated at the Josephson resonance peaks for efficient readout, Figure 5b details a section of Figure 5a between the two quasi-particle peaks (JQP and DJQP). In addition to the magnification, Figure 5b shows how the sensitivity of the rf-SET varies with source - drain and gate bias. The measurement was performed by adding a small square wave signal to the dc gate bias. The intensity plot shows the regions for which source-drain bias and gate voltage yield maximum sensitivity, in this case where the small signal square wave produces a large depth of modulation. We find, that the sensitivity is maximised on the edge of the DJQPs (in gate voltage) with a source-drain bias corresponding to the DJQP resonance. Since we are able to independently bias the two SETs, we are therefore able to operate both SETs under optimum conditions.

VI. CONCLUSION

In conclusion we have described the development of a twin rf-SET device that makes use of two tuned impedance transformers to perform wavelength division multiplexing (WDM) using a single cryogenic following amplifier. In conjunction with a heterodyne demodulation technique, we have explored the issues affecting cross-talk and sensitivity. The twin rf-SET has been shown to perform real time cross-correlation of SET signals. Such a correlation technique suppresses charge noise and enables true signals associated with readout to be distinguished from spurious artifacts on time-scales required for solid state quantum computation. Finally, we have explored the operation of the superconducting rf-SET biased at Josephson resonance peaks where efficient qubit readout is possible. Future work will investigate the use of the twin rf-SET for charge motion detection on microsecond timescales, and its application to read-

out of both semiconducting and superconducting charge qubits.

We thank D. Barber for technical support and S. Kenyon, K. Lehnert and R. Schoelkopf for fruitful discussions and insights. This work was supported by the Australian Research Council, the Australian Government

and by the US National Security Agency (NSA), Advanced Research and Development Activity (ARDA) and the Army Research Office (ARO) under contract number DAAD19-01-1-0653. DJR acknowledges a Hewlett-Packard Fellowship.

-
- [1] J. Preskill, *Proc. R. Soc. Lond. A* **454**, 385 (1998).
- [2] P. W. Shor, *Proceedings, 35th Annual Symposium of Computer Science*, IEEE Press, Los Alamitos, CA (1994).
- [3] B. E. Kane, *Nature* **393**, 133 (1998).
- [4] A. Shnirman, G. Schoenand, and Z. Hermon, *Phys. Rev. Lett.* **79**, 2371 (1997).
- [5] R. Vrijen, E. Yablonovitch, K. Wang, H. Jiang, A. Balandin, V. Roychowdhury, T. Mor, and D. DiVincenzo, *Phys. Rev. A* **62**, 012306 (2000).
- [6] M. H. Devoret and R. J. Schoelkopf, *Nature (London)* **406**, 1039 (2000).
- [7] G. Johansson, A. Kack, and G. Wendin, *Phys. Rev. Lett.* **88**, 046802 (2002).
- [8] A. Aassime, G. Johansson, G. Wendin, R. J. Schoelkopf, and P. Delsing, *Phys. Rev. Lett.* **86**, 3376 (2001).
- [9] R. J. Schoelkopf, P. Wahlgren, A. A. Kozhevnikov, P. Delsing, and D. E. Prober, *Science* **280**, 1238 (1998).
- [10] T. M. Buehler, D. J. Reilly, R. Brenner, A. R. Hamilton, A. S. Dzurak, and R. G. Clark, *Appl. Phys. Lett.* **82**, 577 (2003).
- [11] H. Grabert and M. H. Devoret, *NATO Adv. Study Inst. Ser., Ser. B* **294** (1992).
- [12] T. Fulton, P. Gammel, D. Bishop, L. Dunkelberger, and G. Dolan, *Phys. Rev. Lett.* **63**, 1310 (1989).
- [13] A. A. Clerk, S. M. Girvin, A. Nguyen, and A. D. Stone, *Phys. Rev. Lett.* **89**, 176804 (2002).
- [14] G. Johansson, P. Delsing, K. Bladh, D. Gunnarsson, T. Duty, A. Käck, G. Wendin, and G. Wendin, and A. Aassime (cond-mat/0210163).
- [15] T. Fujisawa and Y. Hirayama, *Appl. Phys. Lett.* **77**, 543 (2000).
- [16] M. Muck, *IEEE Trans. Magn.* **27**, 2986 (1991).
- [17] T. R. Stevenson, F. A. Pellerano, C. M. Stahle, K. Aidala, and R. J. Schoelkopf, *Appl. Phys. Lett.* **80**, 3012 (2002).
- [18] D. M. Pozar, *Microwave Engineering* (Wiley) (1998).
- [19] T. A. Fulton and G. J. Dolan, *Phys. Rev. Lett.* **59**, 109 (1987).
- [20] A. Aassime, D. Gunnarsson, K. Bladh, and Delsing, *Appl. Phys. Lett.* **79**, 4031 (2001).
- [21] D. V. Averin, A. N. Korotkov, A. J. Manninen, and J. P. Pekola, *Phys. Rev. Lett.* **78**, 4821 (1997).